Acta Crystallographica Section D
**Biological Crystallography**
ISSN 0907-4449

# Structure of human TSG101 UEV domain

**Andres Palencia,[a] Jose C. Martinez,[a] Pedro L. Mateo,[a] Irene Luque[a]* and Ana Camara-Artigas[b]***

[a]Department of Physical Chemistry and Institute of Biotechnology, Faculty of Sciences, University of Granada, 18071 Granada, Spain, and [b]Department of Physical Chemistry, Biochemistry and Inorganic Chemistry, University of Almeria, 04120 Almeria, Spain

Correspondence e-mail: iluque@ugr.es, acamara@ual.es

Received 28 November 2005
Accepted 13 February 2006

**PDB Reference:** human TSG101 UEV domain, 2f0r, r2f0rsf.

The UEV domain of the TSG101 protein functions in the vacuolar protein-sorting pathway and in the budding process of HIV-1 and other retroviruses by recognizing ubiquitin in proteins tagged for degradation and short sequences in viral proteins containing an essential and well conserved PTAP motif, respectively. A deep understanding of these interactions is key to the rational design of much-needed novel antivirals. Here, the crystal structure of the TSG101 UEV domain (TSG101-UEV) is presented. TSG101-UEV was crystallized in the presence of PEG 4000 and ammonium sulfate. Under these conditions, crystals were obtained in space group $R3$, with unit-cell parameters $a = b = 97.9$, $c = 110.6$ Å, $\alpha = \beta = 90$, $\gamma = 120^\circ$. Phases were solved by molecular replacement and the crystal structure of TSG101-UEV was refined to an $R$ factor of 18.8% at 2.2 Å resolution. A comparison between the crystal structure and previously reported NMR structures has revealed significant differences in the conformation of one of the loops implicated in ubiquitin recognition. Also, the resulting structure has provided information about the presence of water molecules at the binding interface that could be of relevance for peptide recognition.

## 1. Introduction

Human tumour-susceptibility gene 101 (TSG101) is a member of the class E family of vacuolar protein-sorting proteins and a component of the ESCRT-I complex, which plays an essential role in sorting protein cargo into multivesicular bodies and late endosomal compartments (Lemmon & Traub, 2000; Babst *et al.*, 2000; Katzmann *et al.*, 2001). TSG101 directly interacts with ubiquitin in proteins tagged for degradation through its N-terminal ubiquitin E2 variant (UEV) domain, which binds ubiquitin but lacks ligase activity owing to the absence of the active-site cysteine, which is replaced by a tyrosine residue in the TSG101 sequence (Garrus *et al.*, 2001; Katzmann *et al.*, 2001).

Additionally, the UEV domain of TSG101 (TSG101-UEV) also recognizes short peptide sequences named 'viral late domains' which contain an essential PTAP motif and are found within the gag polyproteins of retroviruses (such as HIV-1 or human T-cell leukaemia virus) and the matrix proteins of filoviruses (Ebola; Freed, 2002). Viral PTAP peptide motifs interact with a hydrophobic groove in the UEV domain of TSG101 adjacent to the ubiquitin-binding site, which in E2 enzymes is occupied by a C-terminal helix that is absent in TSG101 (Pornillos *et al.*, 2002). The different location of the two interaction sites allows the simultaneous or even cooperative binding of ubiquitin and the structural viral proteins (Sundquist *et al.*, 2004).

There is compelling evidence indicating that the recognition of PTAP late domains by TSG101-UEV is essential for recruitment of the cellular endosomal protein-sorting machinery to the viral site of budding, which is in turn critical for the efficient release of viral particles from the infected cell (Martin-Serrano *et al.*, 2001; Demirov *et al.*, 2002; Garrus *et al.*, 2001). As a consequence, the development of small molecules that could block these interactions and impair virus budding is emerging as a new strategy for the discovery of much-needed new broad-spectrum antivirals. In this context, any advances in the structural characterization of the proteins and complexes that could lead to a better understanding of the molecular interactions between TSG101-UEV and its ligands would be of great value for the rational design of high-affinity and high-specificity inhibitors of therapeutic interest.

To date, the high-resolution structures of the TSG101 UEV domain and its complex with a short peptide containing the sequence for the HIV-1 PTAP late domain have been solved by means of NMR techniques (Pornillos, Alam, Davis *et al.*, 2002; Pornillos, Alam, Rich *et al.*, 2002). Recently, the crystallographic structure of TSG101-UEV in complex with ubiquitin has also been reported (Sundquist *et al.*, 2004). Here, we present the X-ray structure of the unliganded TSG101 UEV domain. Significant differences in the conformation of some loops that are important for the recognition of ubiquitin have been observed in comparison with the solution structures of TSG101-UEV; however, the conformational changes elicited upon ubiquitin recognition that were initially proposed based on the comparison between the X-ray structure of the TSG101-UEV–ubiquitin complex and the NMR structure of the free protein (Teo *et al.*, 2004) are not apparent when comparing the two crystal structures. The possible origins of these differences as well as additional information concerning intermolecular contacts and water molecules of possible relevance for ligand recognition are further discussed.

## 2. Experimental procedures

### 2.1. Protein purification and crystallization

The plasmid pRSETA containing the TSG101-UEV domain was a generous gift from Dr W. Weissenhorn (EMBL, Grenoble). The TSG101-UEV domain (1–145) gene, coding for the sequence *MRGSHHHHHHG* $M_1$ASMAVSESQ-LKKMVSKYKYRDLTVRETVNVITLYKDLKPVLDSYV-FNDGSSRELMNLTGTIPVPYRGNTYNIPICLWLLDTYP-YNPPICFVKPTSSMTIKTGKHVDANGKIYLPYLHEWK-HPQSDLLGLIQVMIVVFGDEPPVFSRP$_{145}$, was expressed in *Escherichia coli* BL21 (DE3) Codon Plus cells (Novagen). Briefly, 100 ml Luria–Bertani (LB) medium with ampicillin and chloramphenicol was inoculated with a colony of cells and incubated at 310 K overnight. 10 ml of the resulting overnight culture was added to 1 l LB medium and grown at 310 K. Once the optical density of the culture reached a value of 0.8 at 600 nm, protein expression was induced with 1 m*M* isopropyl $\beta$-D-thiogalactopyranoside (IPTG). After 4 h of growth, cells were harvested by centrifugation at 277 K and resuspended in 50 m*M* sodium phosphate, 300 m*M* sodium chloride and 5 m*M* $\beta$-mercaptoethanol pH 8.0 buffer (column buffer; CB). The cells were broken in a French pressure cell and ultracentrifugated for 30 min at 12 000*g*. The cleared supernatant was loaded onto 5 ml Ni–NTA resin (Qiagen) previously equilibrated with CB and was extensively washed with CB, CB plus 20 m*M* imidazole and CB plus 50 m*M* imidazole. The protein was eluted with CB plus 500 m*M* imidazole. Protein-containing fractions were extensively dialyzed against 50 m*M* glycine pH 3.0 to remove imidazole, concentrated to 5 mg ml$^{-1}$ and stored at 193 K. Protein purity was checked by SDS–PAGE and matrix-assisted laser desorption/ionization time-of-flight (MALDI–TOF) mass spectrometry. A single peak at $m/z$ = 18 238 (sodium adduct) was obtained. Protein concentration was determined spectroscopically by absorbance measurements at 280 nm, using an extinction coefficient of 24 180 $M^{-1}$ cm$^{-1}$ determined by the method of Gill & von Hippel (1989) and a molecular weight of 18 215 kDa.

The purified protein was dialyzed into crystallization buffer (50 m*M* glycine pH 3.0) and was concentrated to approximately 10 mg ml$^{-1}$ using a Microcon YM-10. Crystallization conditions were identified using Crystal Screen I and II reagent kits (Hampton Research). Crystallization was performed using the hanging-drop vapour-diffusion method at 288 K in 48-well plates. 2 µl protein solution was mixed with 2 µl reservoir solution and equilibrated against 200 µl reservoir solution.

Three different conditions from Crystal Screen I were found to yield microcrystals: condition No. 9 (30% PEG 4000, 0.2 *M* ammonium sulfate, 0.1 *M* sodium citrate pH 5.6), condition No. 15 (30% PEG 8000, 0.2 *M* ammonium sulfate, 0.1 *M* sodium cacodylate pH 6.5) and condition No. 16 (1.5 *M* lithium sulfate, 0.1 *M* HEPES pH 7.5). After optimization of the crystallization conditions, the best crystals were obtained in 20% PEG 4000, 0.2 *M* ammonium sulfate, 0.1 *M* Tris pH 8.0. As a standard crystallization procedure, 10 µl droplets were prepared by mixing 5 µl protein solution and 5 µl reservoir solution. The mixture was vapour-equilibrated against 500 µl reservoir solution. Under these conditions, small crystals typically appeared after one week and the size of the crystals reached approximately 0.8–1 mm after 1–2 months (Fig. 1).

### 2.2. X-ray data collection and processing

Crystals were gradually transferred to a mother-liquor solution containing a final concentration of 10% glycerol. The mounted crystal was then placed in a cold nitrogen stream (Kryoflex) maintained at 110 K. A total of 500 frames of 0.5° oscillation images were collected for each data set with a Bruker Microfocus (Montel Optics) Microstar rotating-anode X-ray generator operated at 45 kV and 60 mA with $\kappa$ configuration and a Proteum X8 CCD detector. Integrated intensity information for each reflection was obtained with the program *SAINT* and scaled with the *SADABS* module of the *PROTEUM* suite. The best crystal diffracted to 2.25 Å resolution and belonged to space group *R*3, with unit-cell para-

**Table 1**
Data-collection and processing statistics.

Values in parentheses are for the highest resolution bin.

| | |
|---|---|
| Space group | *R*3 |
| Unit-cell parameters | |
| *a* (Å) | 97.9 |
| *b* (Å) | 97.9 |
| *c* (Å) | 110.6 |
| Resolution (Å) | 60–2.25 |
| Total observations | 101426 |
| Unique reflections | 17160 |
| Completeness | 92.4 (64.7) |
| $I/\sigma(I)$ | 26.3 (2.4) |
| $R_{\rm merge}$† | 0.04 (0.44) |
| Protein residues | 143 |
| *R* (%) | 18.9 |
| $R_{\rm free}$ (%) | 24.3 |
| R.m.s.d. from ideal geometry | |
| Bonds (Å) | 0.020 |
| Angles (°) | 1.785 |
| Average *B* factors (Å$^2$) | |
| Main chain | 36.8 |
| Side chain | 37.3 |

† $R_{\rm merge} = \sum_{hkl}\sum_i |I_i - \langle I\rangle|/|\langle I\rangle|$, where $I_i$ is the intensity for the *i*th measurement of an equivalent reflection with indices *hkl*.

meters $a = b = 97.9$, $c = 110.6$ Å, $\alpha = \beta = 90.00$, $\gamma = 120.00°$. The Matthews coefficient is 3.2 Å$^3$ Da$^{-1}$ with a solvent content of 61.1% and 2.1 Å$^3$ Da$^{-1}$ with a solvent content of 41.6% for two and three TSG101 molecules in the asymmetric unit, respectively (Matthews, 1968). The crystallographic parameters and statistics of the data collection are listed in Table 1.

### 2.3. Structure resolution

Initial phasing was obtained with *MOLREP* (Vagin & Teplyakov, 1997) using the coordinates for the TSG101 UEV domain from the previously reported structure of the TSG101-UEV–ubiquitin complex (PDB code 1s1q) as the model. The ubiquitin chain and the water molecules were removed from the molecular-replacement model. Only two large peaks were obtained for the rotation function. The translation function together with the packing function yielded two TSG101 molecules in the asymmetric unit with an initial *R* factor of 38.8%.

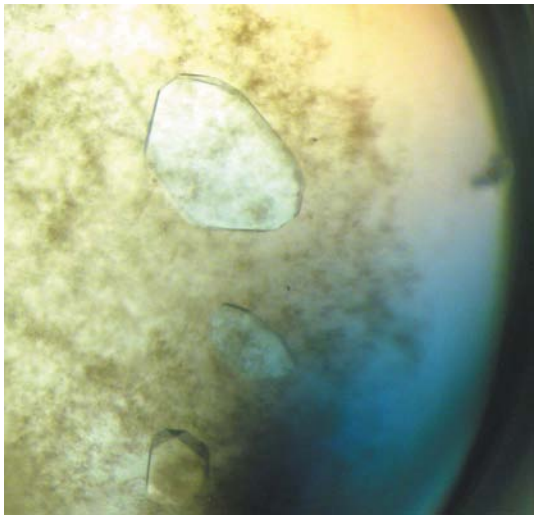

**Figure 1**
Crystals of human TSG101 UEV protein. Crystals were grown in 0.1 *M* Tris, 20% PEG 4000 and 0.2 *M* ammonium sulfate pH 8.

### 2.4. Structure refinement and model building

The two molecules found in the asymmetric unit are related by a twofold axis that does not correspond to the crystallographic twofold axis present in space group *R*32. The earliest stages of the structure refinement were carried out using the *CNS* program package (Brünger *et al.*, 1998). Two molecules in the asymmetric unit were constrained with strict NCS (Weis *et al.*, 1990). After rigid-body refinement, several cycles of restrained positional and temperature-factor refinement using the resolution range 30–2.2 Å were alternated with manual building using the resulting $\sigma_A$-weighted $2F_o - F_c$ and $F_o - F_c$ electron-density maps and the *O* suite (Jones *et al.*, 1991). To avoid model bias, an annealing omit map was used. Once the model reached an *R*-factor value of 30.1% ($R_{\rm free}$ = 31.9%), the final step of the refinement was carried out with *REFMAC*5 using the TLS parameters (Winn *et al.*, 2001) defined for each of the two TSG101 UEV domain molecules in the asymmetric unit. The inclusion of TLS parameters in the refinement clearly improves the *R* and $R_{\rm free}$ factors (10% lower). Water molecules were placed in the residual electron density using the *ARP*/*wARP* v.5.0 program from the *CCP*4 suite (Collaborative Computational Project, Number 4, 1994). The final model contains two chains with 143 amino-acid residues and 243 solvent molecules with an *R* factor of 18.8% ($R_{\rm free}$ = 24.3%).

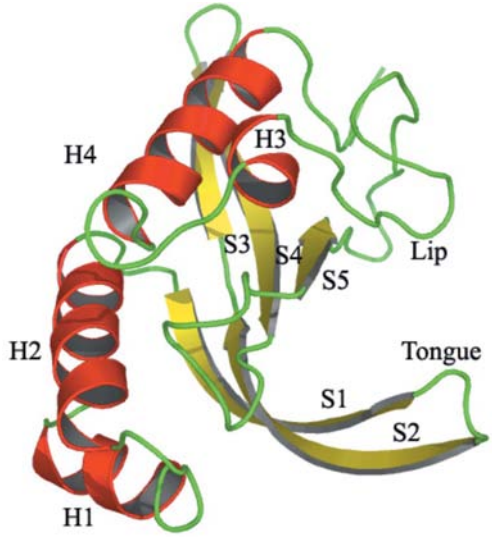


**Figure 2**
Ribbon representation of the crystal structure of the human TSG101 UEV domain. β-Strands are coloured yellow and labelled S1–S5 and α-helices are coloured red and labelled H1–H3. Loops important for ubiquitin recognition are labelled 'lip' and 'tongue'.

## 3. Results and discussion

### 3.1. Model quality and overall fold

The statistics of the TSG101-UEV model are summarized in Table 1. Two molecules have been built in the asymmetric unit, chains *A* and *B*, with an average root-mean-square deviation (r.m.s.d.) of 0.234 Å. No residues in the disallowed regions of the Ramachandran plot were found in any of the chains: 93% of the amino acids are placed in the most favoured regions and only 7% appear in allowed regions. The overall fold is the typical UBC-like structure (SCOP classification) composed of a four-stranded antiparallel $\beta$-sheet and four $\alpha$-helices packed against one face of the sheet (Fig. 2). The first three residues of TSG101 and the preceding His-tag residues are disordered and lack electron density.

Comparison of the resulting structure for the TSG101 UEV domain with the previously reported crystallographic structure in complex with ubiquitin (Sundquist *et al.*, 2004; PDB code 1s1q) reveals that both structures are practically identical, with an r.m.s.d. displacement of only 2 Å that exclusively involves amino acids Asp45 and Asp46 in the $\beta$-hairpin tongue (Fig. 3*a*). Previously, a conformational change involving this region had been proposed based on the comparison between the solution structure of the free TSG101 UEV domain solved by NMR techniques (Pornillos *et al.*, 2003; PDB code 1kpq) and the crystal structure of the ubiquitin complex, which had been solved independently by using seleniomethionine-

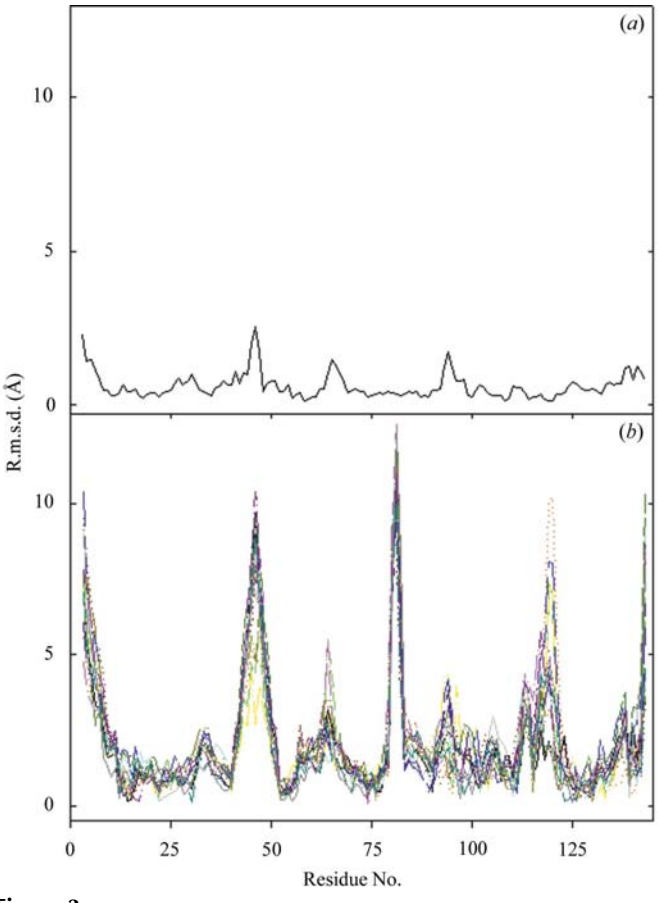


**Figure 3**
Comparison of the various structures available for human TSG101 UEV domain. (*a*) R.m.s.d. plot of chain *A* of the unliganded TSG101 UEV domain (this work) and the TSG101-UEV–ubiquitin complex (PDB code 1s1q). R.m.s.d. values were calculated with the *CCP*4 program. (*b*) R.m.s.d. plot of chain *A* of the unliganded TSG101-UEV domain solved by X-ray crystallography and the NMR structure in solution (PDB code 1kpp; 15 models).

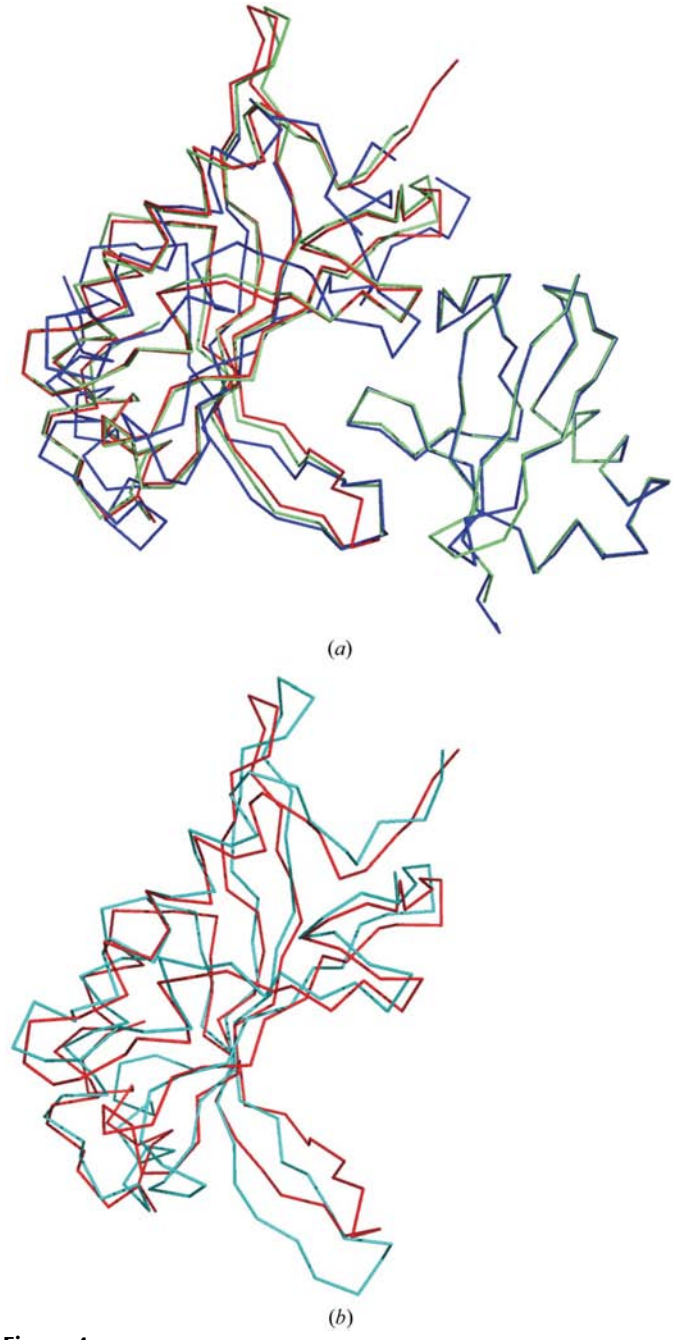


**Figure 4**
Superposition of the various structures available for human TSG101 UEV domain. (*a*) Superposition of the crystallographic structures of the unliganded (red) and ubiquitin-bound (lime; PDB code 1s1q) TSG101 UEV domain together with the homologous Vps23 in complex with ubiquitin (blue; PDB code 1uzx). (*b*) Superposition of the models corresponding to the unliganded TSG101 UEV domain. The X-ray structure (this work) is shown in red and the NMR solution structure (PDB code 1kpq) in cyan.

substituted TSG101-UEV and ubiquitin to obtain phases *via* MAD phasing techniques (Sundquist *et al.*, 2004). The superposition of both structures revealed deviations of up to 10 Å at the 43–49 $\beta$-hairpin loop that were proposed to be of biological significance since this loop is implicated in ubiquitin recognition. However, this conformational change is not observed when comparing the free and ubiquitin-bound crystal structures, in which the $\beta$-hairpin tongue occupies the same conformation (see Fig. 4*a*). Additionally, comparison of the TSG101-UEV crystal structures with the recently solved crystallographic structure of the complex between the UEV domain of Vps23, the yeast homologue of TSG101, and ubiquitin (Teo *et al.*, 2004; PDB code 1uzx) does not reveal significant differences in the 43–49 hairpin region, as is also illustrated in Fig. 4(*a*).

The r.m.s.d. for the superposition of the NMR and crystal structures of the free TSG101 UEV domain is summarized in Fig. 3(*b*) and illustrated in Fig. 4(*b*). The average r.m.s.d. is 0.595 Å, with the most dramatic differences being found in the 43–49 loop, which shows displacements of up to 10 Å. In addition, to avoid bias an annealing omit map was obtained and the electronic density for the $\beta$-hairpin 'tongue' was clear for the entire backbone, only with the side chains of residues 44–46 being weakly defined. It is interesting to note that this region is poorly defined in the solution structure, as indicated by the r.m.s.d. values obtained for the proposed ensemble of NMR models (see Fig. 3*b*), which are of the same magnitude as the differences observed between the X-ray and NMR models. This apparent disorder is not observed in the X-ray structures, in which the *B* factors corresponding to this $\beta$-hairpin region are similar to the structure average values. The higher definition of this region in the crystallographic structures could not be attributed to crystal-packing stabilization effects because the only crystal contact observed is a weak long-range interaction (>3.6 Å) between Asn45 in chain *A* and the symmetry-related Asn45 residue in chain *B*. Also, there is enough room in the crystal packing to allow the loop to freely move to occupy the positions observed in the NMR structures. Recently, Garbuzynskiy *et al.* (2005), in an extensive comparison of X-ray and NMR structures, have postulated the poorer refinement of the NMR models as the possible origin of the discrepancies frequently observed between NMR and X-ray structures. Fig. 3(*b*) also reveals a noticeable displacement between the NMR and X-ray structures for the amino acids in the loops 78–84 and 116–124. Those disagreements are also observed when comparing the NMR structures of the unliganded Tsg101 UEV domain and the complex with a peptidic ligand containing the PTAP late domain present in the p6 region of the HIV-1 GAG polyprotein. In order to compare the quality of TSG101-UEV domain NMR and X-ray models, we used the *MOLPROBITY* web service (Richardson *et al.*, 2003; http://kinemage.biochem.duke.edu/molprobity/). From the analysis, we obtained a Ramachandran plot for the X-ray model that shows 93% of the residues in the most favoured regions, while the average NMR model has only 73%. Furthermore, the outlier rotamers for the 15 NMR models range from 25 to 38%, which is far above the recommended value of less than 1%.

### 3.2. Crystal packing and contacts

The crystal structure of the TSG101 UEV domain shows a noncrystallographic symmetry dimer in the asymmetric unit that is generated by a twofold screw axis almost parallel to the *x* axis. The dimerization interface between the two subunits (*A* and *B*) mainly involves $\alpha$-helices 2 and 4 and buries a total surface of 1360 Å$^2$ (870.1 Å$^2$ of non-polar surface and 490.2 Å$^2$ of polar surface), which is about 15% of the total solvent-accessible surface per subunit. The areas implicated in the dimerization interface are markedly hydrophobic. Judging by the size of the buried surface, it is not likely that the observed dimerization interface has physiological relevance. Furthermore, this protein is a structural domain of TSG101, which makes this possibility improbable. The observed dimer in the crystal is likely to be promoted by the high salt concentration in the precipitant solution rather than corresponding to a thermodynamically stable interaction in solution between the hydrophobic patches at the surface of the protein (Janin & Rodier, 1995). In addition, dimer formation increases the globularity of the protein, favouring crystal packing. Accordingly, no experimental evidence for dimerization of TSG101-UEV in solution has been observed. MALDI–TOF experiments show that our protein is a monomer in solution, characterized by an apparent molecular weight of 18 238 Da (sodium adduct), which is in good agreement with the expected molecular weight for the monomeric species. Furthermore, our ligand-binding studies carried out by isothermal titration calorimetry corroborate this observation (Palencia *et al.*, 2006).

Additionally, another intermolecular hydrophobic interaction is observed in the carboxy-terminal region of the protein, where Pro145 is in contact with residues Tyr63, Tyr68, Pro139 and Val141 of the symmetry-related molecule. The other crystal contacts observed between neighbouring molecules are all hydrophilic in nature. Interestingly, next to a broad positively charged patch, a large electronic density peak ($\sigma > 7$) was found in both $2F_o - F_c$ and $F_o - F_c$ maps, into which two sulfate ions have been modelled. The first of these ions is placed in a crystal contact bridging residues Lys9, Lys16, Arg18 and Asp19 in chain *B* with residue Lys118 in chain *A* of the symmetry-related molecule. The second sulfate ion is coordinated by the corresponding residues in chain *A*, but in this case the contact with Lys118 in chain *B* of a symmetry-related molecule is mediated by two water molecules. These sulfate ions are also present in the TSG101-UEV–ubiquitin complex structure that was crystallized with sulfate in the precipitant solution (Sundquist *et al.*, 2004). However, in this structure neither of these ions participates in any crystal contacts.

### 3.3. Water molecules

One important advantage of X-ray crystallography over NMR techniques is that at moderate resolution (2.5 Å) it

allows accurate modelling of solvent. Water molecules can play an important role in protein recognition as long-lived buried water molecules are frequently found at the binding interface in protein–protein and protein–ligand complexes (Barratt *et al.*, 2005; Andujar-Sanchez *et al.*, 2005; Wang *et al.*, 1996; Wang & Ben-Naim, 1996).

A total of 15 ordered water molecules were found buried at the binding interface in the crystal structure of the complex between the TSG101 UEV domain and ubiquitin, establishing a complex hydrogen-bond network and bridging important interactions in the complex (Sundquist *et al.*, 2004). A thermodynamic analysis of the interaction between TSG101 UEV domain and several PTAP peptides reveals that this interaction is characterized by a similar thermodynamic signature to that described for SH3 domains (Palencia *et al.*, 2004), which suggests that water molecules at the interface also play a role in these interactions (Palencia *et al.*, 2006). In this respect, two water molecules have been found at the PTAP-binding site in the structure of the unliganded TSG101 UEV domain that could remain in the complex. These water molecules are in contact with residues Ser143 and Arg144 which, according to the NMR structure for the TSG101-UEV–HIV1 peptide, could play a role in bridging the interaction with the $O^{\gamma}$ donor from the threonine residue in the peptide. Accurate knowledge of the presence and position of fixed water molecules in the free and complexed structures is of great interest for the rational design of improved high-affinity ligands with potential therapeutic value as broad-spectrum antivirals.

## 4. Summary

The crystallographic high-resolution structure of the UEV domain from TSG101 is presented. Comparison with the previously determined solution structure reveals important differences that are mostly related to the position of the $\beta$-hairpin tongue, which is implicated in ubiquitin recognition. In light of the crystal structure and considering that the r.m.s.d. deviations between the crystal structure of the ubiquitin complex and the NMR structure of the unliganded protein are of the same magnitude as the dispersion within the set of NMR models, a previously proposed conformational change coupled to ubiquitin binding is not apparent. Additionally, the structures of TSG101-UEV and its yeast homologue Vps23-UEV in complex with ubiquitin show only small changes (<3 Å) in this loop. The crystal structure presented in this work has provided information about the presence of fixed water molecules at the binding sites that is potentially relevant for the interactions of TSG101-UEV with ligands, which could be of importance for future rational design strategies.

This work was funded by grants BIO2003-04274 from the Spanish Ministry of Science and Technology and 03-51-5569 INTAS from the European Union and grants to the research teams FQM-171 and CVI-292 from the Andalusian Government. AP was supported by a pre-doctoral research contract funded by the Spanish Ministry of Education and Sciences. IL is the recipient of a Ramon y Cajal Research contract from the Spanish Ministry of Education and Sciences. We thank Dr Winfried Weissenhorn (EMBL, Grenoble) for generously providing us with the expression vector for the TSG101 UEV domain. We thank the research group of J. M. García-Ruiz and particularly Dr J. A. Gavira for technical assistance with data collection at the Laboratorio de Estudios Cristalograficos (CSIC). We also thank the mass-spectrometry service (Scientific Instrumentation Center) at the University of Granada.

## References

Andujar-Sanchez, M., Smith, A. W., Clemente-Jimenez, J. M., Rodriguez-Vico, F., LasHeras-Vazquez, F. J., Jara-Perez, V. & Camara-Artigas, A. (2005). *Biochemistry*, **44**, 1174–1183.
Babst, M., Odorizzi, G., Estepa, E. J. & Emr, S. D. (2000). *Traffic*, **1**, 248–258.
Barratt, E., Bingham, R. J., Warner, D. J., Laughton, C. A., Phillips, S. E. V. & Homans, S. W. (2005). *J. Am. Chem. Soc.* **127**, 11827–11834.
Brünger, A. T., Adams, P. D., Clore, G. M., DeLano, W. L., Gros, P., Grosse-Kunstleve, R. W., Jiang, J.-S., Kuszewski, J., Nilges, M., Pannu, N. S., Read, R. J., Rice, L. M., Simonson, T. & Warren, G. L. (1998). *Acta Cryst.* D**54**, 905–921.
Collaborative Computational Project, Number 4 (1994). *Acta Cryst.* D**50**, 760–763.
Demirov, D. G., Ono, A., Orenstein, J. M. & Freed, E. O. (2002). *Proc. Natl Acad. Sci. USA*, **99**, 955–960.
Freed, E. O. (2002). *J. Virol.* **76**, 4679–4687.
Garbuzynskiy, S. O., Melnik, B. S., Lobanov, M. Y., Finkelstein, A. V. & Galzitskaya, O. V. (2005). *Proteins*, **60**, 139–147.
Garrus, J. E., von Schwendler, U. K., Pornillos, O. W., Morham, S. G., Zavitz, K. H., Wang, H. E., Wettstein, D. A., Stray, K. M., Cote, M., Rich, R. L., Myszka, D. G. & Sundquist, W. I. (2001). *Cell*, **107**, 55–65.
Gill, S. C. & von Hippel, P. H. (1989). *Anal. Biochem.* **182**, 546–551.
Janin, J. & Rodier, F. (1995). *Proteins*, **23**, 580–587.
Jones, T. A., Zou, J.-Y., Cowan, S. W. & Kjeldgaard, M. (1991). *Acta Cryst.* A**47**, 110–119.
Katzmann, D. J., Babst, M. & Emr, S. D. (2001). *Cell*, **106**, 145–155.
Lemmon, S. K. & Traub, L. M. (2000). *Curr. Opin. Cell Biol.* **12**, 457–466.
Martin-Serrano, J., Zang, T. & Bieniasz, P. D. (2001). *Nature Med.* **7**, 1313–1319.
Matthews, B. W. (1968). *J. Mol. Biol.* **33**, 491–497.
Palencia, A., Cobos, E. S., Mateo, P. L., Martinez, J. C. & Luque, I. (2004). *J. Mol. Biol.* **336**, 527–537.
Palencia, A., Martinez, J. C., Mateo, P. L. & Luque, I. (2006). In preparation.
Pornillos, O., Alam, S. L., Davis, D. R. & Sundquist, W. I. (2002). *Nature Struct. Biol.* **9**, 812–817.
Pornillos, O., Alam, S. L., Rich, R. L., Myszka, D. G., Davis, D. R. & Sundquist, W. I. (2002). *EMBO J.* **21**, 2397–2406.
Pornillos, O., Higginson, D. S., Stray, K. M., Fisher, R. D., Garrus, J. E., Payne, M., He, G.-P., Wang, H. E., Morham, S. G. & Sundquist, W. I. (2003). *J. Cell Biol.* **162**, 425–434.
Richardson, J. S., Arendall, W. B. & Richardson, D. C. (2003). *Methods Enzymol.* **374**, 385–412.
Sundquist, W. I., Schubert, H. L., Kelly, B. N., Hill, G. C., Holton, J. M. & Hill, C. P. (2004). *Mol. Cell*, **13**, 783–789.
Teo, H., Veprintsev, D. B. & Williams, R. L. (2004). *J. Biol. Chem.* **279**, 28689–28696.
Vagin, A. & Teplyakov, A. (1997). *J. Appl. Cryst.* **30**, 1022–1025.

Wang, H. & Ben-Naim, A. (1996). *J. Med. Chem.* **39**, 1531–1539.
Wang, Y.-X., Freedberg, D. I., Wingfield, P. T., Stahl, S. J., Kaufman, J. D., Kiso, Y., Bhat, T. N., Erickson, J. W. & Torchia, D. A. (1996). *J. Am. Chem. Soc* **118**, 12287–12290.
Weis, W. I., Brünger, A. T., Skehel, J. J. & Wiley, D. C. (1990). *J. Mol. Biol.* **212**, 737–761.
Winn, M. D., Isupov, M. N. & Murshudov, G. N. (2001). *Acta Cryst.* D**57**, 122–131.